Comparison of Brain Tumor Contrast-enhancement on T_1-CUBE and 3D-SPGR Images

Mungunkhuyag Majigsuren[1], Takashi Abe[1], Teruyoshi Kageji[2], Kenji Matsuzaki[1],

Mayumi Takeuchi[1], Seiji Iwamoto[1], Yoichi Otomi[1], Naoto Uyama[1],

Shinji Nagahiro[2], and Masafumi Harada[1*]

[1]Department of Radiology, Institute of Health Biosciences, The University of Tokushima Graduate School

3-18-15, Kuramoto-cho, Tokushima City, Tokushima, 770-8509, Japan

[2]Department of Neurosurgery, Institute of Health Biosciences, The University of Tokushima Graduate School

[*]Corresponding author, Phone: +81-88-633-9283, Fax: +81-88-633-7174, E-mail: masafumi@tokushima-u.ac.jp

Running head: Brain Tumor CE on T_1-Cube versus 3D SPGR

Abstract

Purpose: T_1-Cube (GE HealthCare) is a relatively new 3-dimensional (3D) fast spin-echo (FSE)-based magnetic resonance (MR) imaging sequence that uses a variable flip angle to acquire gap-free volume scans. We compared the gadolinium enhancement characteristics of a heterogeneous population of brain tumors imaged by T_1-Cube and then 3D fast spoiled gradient recall acquisition in steady state (3D FSPGR) 3-tesla MR imaging to identify the superior modality for specific diagnostic purposes.

Methods: We examined 61 lesions from 32 patients using the 2 sequences after administration of gadopentetic acid (Gd-DTPA; 0.1 mmol/kg). Two neuroradiologists independently measured each lesion twice using a region-of-interest (ROI) method. We measured the contrast-to-noise ratio (CNR), the difference in signal intensity (SI) between the tumor and normal white matter relative to the standard deviation (SD) of the SI within the lesion, for both post-contrast 3D FSPGR and post-contrast T_1-Cube images of the same tumor and compared modality-specific CNRs for all tumors and in subgroups defined by tumor size, enhancement ratio, and histopathology.

Results: The mean CNR was significantly higher on T_1-Cube images than 3D FSPGR images for the total tumor population (1.85 ± 0.97 versus 1.12 ± 1.05, $P < 0.01$) and the histologic types, i.e., metastasis ($P < 0.01$) and lymphoma ($P < 0.05$). The difference in CNR was even larger for smaller tumors in the metastatic group (4.95 to 23.5 mm^2) ($P < 0.01$). In contrast, mean CNRs did not differ between modalities for high grade glioma and meningioma.

Conclusions: Gadolinium enhancement of brain tumors was generally higher when imaged by T_1-Cube than 3D FSPGR, and T_1-Cube with Gd enhancement may be superior to 3D FSPGR for detecting smaller metastatic tumors.

Introduction

Two-dimensional (2D) contrast-enhanced magnetic resonance imaging (CE MRI) using T_1-weighted spin-echo (SE) or 3-dimensional (3D) gradient-echo (GRE) sequences is the most common imaging modality for detecting and evaluating brain tumors.(1-3) Previous studies, however, reported better visualization of small tumors by thin 3D GRE images, such as 3D fast spoiled gradient recall acquisition in the steady state (3D FSPGR), than by conventional 2D T_1-weighted SE images.(1,4) Indeed, 3D T_1-weighted GRE imaging with high spatial resolution can be advantageous for detecting small enhancing brain tumors because it minimizes partial volume effects.(4-6) On the other hand, Furutani's group(1) reported lower enhancement on 3D FSPGR images than conventional 2D T_1-weighted SE images, even with 3-T MR imaging, indicating that thin-slice CE 2D T_1-weighted SE images may be preferable for the detection of smaller tumors and brain metastasis.

T_1-Cube is a relatively new 3D T_1-weighted fast spin-echo (FSE) sequence that uses a variable flip angle technique and higher echo train length to reduce acquisition time and specific absorption rate. This allows T_1-Cube imaging to provide submillimeter, isotropic 3D data sets that can be reformatted into any plane to visualize even small and low-contrast lesions without partial-volume effects.(7,8) In fact, the similar "sampling perfection with application-optimized contrasts by using different flip angle evolutions" (SPACE) sequence has proven advantageous for detecting brain metastasis compared with 3D T_1-weighted GRE sequences.(9,10) In this study, we compared post-contrast T_1-Cube and 3D FSPGR images of the same brain tumors to identify advantages and limitations of these modalities for analysis of specific brain tumor subgroups defined by size, degree of enhancement, and histopathological type.

Materials and Methods

This study was approved by our institutional review board and prospectively performed after acquisition

of informed consent from all patients.

Imaging protocols

All MR examinations were performed using a 3-T MR scanner (Discovery 750, GE HealthCare,

Milwaukee, WI, USA) and standard 8-channel head coil. We obtained 3D FSPGR (sagittal), T_2-weighted

(axial), and diffusion-weighted (axial) images prior to contrast administration and acquisition of post-contrast

T_1-Cube and 3D FSPGR images in the sagittal plane. Four minutes after injection of a gadolinium contrast

agent (gadopentetic acid [Gd-DTPA], 0.1 mmol/kg, Magnevist, Bayer HealthCare, Germany) with a power

injector (Medrad®, Indianola, PA, USA) at 2.5 mL/s followed by a 20-mL saline flush at the same rate, T_1-

Cube was performed, and post-contrast 3D FSPGR images were acquired immediately following completion

of T_1-Cube measurements. Scan parameters for T_1-Cube were: repetition time (TR)/echo time (TE), 500

ms/15.1 ms; bandwidth, 50 kHz; slice thickness, 1.2 mm; matrix 384×256; echo train length, 18; flip angle,

15º; number of excitations (NEX), one; field of vision (FOV), 24×24 cm; acceleration factor, 2×2; number

of slices, 160; and scan time 4 minutes 5 seconds. Scan parameters for 3D FSPGR were: TR/TE, 10.4 ms/4.4

ms; bandwidth, 31.25 kHz; slice thickness, 1.2 mm; matrix, 384×256; flip angle, 15º; NEX, one; FOV, $24 \times$

24 cm; acceleration factor, 2×2; number of slices, 160; and scan time, 3 minutes 34 seconds. All MR

examinations were performed before conducting any antitumor therapy.

Patients

We considered for study 54 consecutive patients who underwent contrast-enhanced MR imaging for diagnosis of suspected brain tumors between December 10, 2012 and February 24, 2014. Two neuroradiologists (M.M., T.A.) unaware of the final diagnosis of the lesion chose all enhanced lesions for image analysis. Lesions smaller than 3 mm^2 were excluded. The diagnosis was made pathologically or radiologically by the consensus of 4 experienced radiologists with 10 to 16 years of experience in neuroimaging (M.T., S.I., Y.O., N.U.). Ultimately, we selected 32 patients (17 men, 15 women; mean age, 63.1 years; age range, 34 to 84 years) for study, including 9 patients with metastasis (34 lesions), 11 with high grade glioma (HGG, 13 lesions), 4 with primary central nervous system (CNS) lymphoma (6 lesions), and 8 with meningioma (7 meningiomas and one hemangiopericytoma). Tumor specimens of 30 of the 32 patients were obtained during surgery and stained with hematoxylin-eosin for histopathological evaluation by an experienced neuropathologist blinded to the imaging findings. Table 1 summarizes patient data.

Data analysis

We analyzed pre-contrast 3D FSPGR, post-contrast 3D FSPGR, and post-contrast T_1-Cube images on an Advantage workstation (AW 4.6) (GE HealthCare, Milwaukee, WI). Two neuroradiologists with 10 (M.M.) and 25 years (M.H.) of experience in neuroimaging independently measured each lesion using a region-of-interest (ROI) method. Both examiners measured the lesions twice (in the same plane and at the same anatomic level) during 2 sessions separated by at least 2 weeks. The order of cases was randomized during each session. For the first measurement of enhanced T_1-Cube images, a hand-drawn polygonal ROI was

defined as large as possible to include necrotic areas of the lesion. This digital ROI was then copied to the

corresponding pre- and post-contrast 3D FSPGR images. For the second measurement (about 2 weeks later), a

polygonal ROI was first drawn on the post-contrast 3D FSPGR and then copied to the corresponding post-

contrast T_1-Cube and pre-contrast 3D FSPGR images. The mean signal intensity (SI) and area of the ROI were

measured for each tumor. Another ROI, approximately 100 mm^2, was drawn on normal-appearing white

matter (WM) as a reference value for calculating the contrast-to-noise ratio (CNR). Figure 1 illustrates these

measurement parameters.

Statistical analysis

We expressed contrast enhancement using the CNR,(9,11,12) defined as: CNR = (SI_{lesion} - SI_{white}

$_{matter}$)/SD_{lesion}, in which SI_{lesion} represents the mean SI value of the lesion, $SI_{white\ matter}$ is that of surrounding

normal-appearing white matter, and SD_{lesion} is the standard deviation of the SI within the lesion. For both

measurements, we used the intraclass correlation coefficient (ICC) to estimate inter-rater reliability. We used

Spearman's rank correlation to evaluate the relationship between CNR and tumor size for both post-contrast

T_1-Cube and post-contrast 3D FSPGR images and the Wilcoxon rank sum test to compare CNRs and

subgroups between imaging modalities.

All statistical analysis was performed using Excel Statistics 2012 (Social Survey Research Information

Co., Ltd., Tokyo, Japan) and Excel 2010 (Microsoft Co., Redmond, WA, USA). *P* < 0.05 was considered

significant.

Comparison of CNR and enhancement ratio (ER) by tumor group

We divided the contrast-enhanced lesions into 2 subgroups according to the degree of enhancement or the

ER, namely, $CR_{\text{post-contrast 3D FSPGR}}$ / $CR_{\text{pre-contrast 3D FSPGR}}$, and defined CR as $CR = SI_{\text{lesion}}/ SI_{\text{white matter}}$.(4,10)

We used the median overall ER value (1.97) as the threshold for defining strong and weak enhancement

subgroups. The ER of the strong enhancement group ranged from 1.98 to 2.86 (28 lesions), and the ER of the

weak enhancement group ranged from 1.23 to 1.97 (33 lesions). In the strong enhancement group,

histopathological type distribution was metastasis (n = 11), HGG (n = 7), meningioma (n = 7), and lymphoma

(n = 3). In the weak enhancement group, histopathological type distribution was metastasis (n = 23), HGG (n

= 6), meningioma (n = one), and lymphoma (n = 3). We also analyzed the lesions according to

histopathological subgroup−brain metastasis, HGG, meningioma, and lymphoma.

Comparison of CNR by tumor size in the metastasis group

To examine the relationship between CNR and tumor size, we restricted analysis to the metastatic tumors

because these were the most common. We measured the maximum lesion size according to the enhanced area

on primary sagittal images. Very small metastatic lesions (< 3 mm^2) were excluded from the evaluation

because of insufficient measurement reliability. We divided the metastatic lesions measured into 2 size

subgroups, those larger than the median of 24.2 mm^2 (range, 24.9 to 1949.5 mm^2) and those smaller than the

median (range, 4.95 to 23.5 mm^2).

Results

High inter-rater reliability was confirmed by an intra-class correlation coefficient above 0.9 for both CNR

and tumor size estimates.

Comparison of tumor CNR and size as measured by T_1-Cube or 3D FSPGR

The CNR was significantly higher on T_1-Cube images than 3D FSPGR images for the entire tumor

population (1.85 ± 0.97 versus 1.12 ± 1.05; Wilcoxon test, $P < 0.01$). Furthermore, mean tumor size was

slightly larger on T_1-Cube images than on 3D FSPGR images, although the difference did not reach statistical

significance (315.4 ± 497.4 mm^2 versus 313.1 ± 493.8 mm^2; Wilcoxon test, $P = 0.29$).

Subgroup analyses

Metastatic tumor size

As shown in Table 2, the mean CNR was higher on T_1-Cube images than 3D FSPGR images for the large

metastatic tumors, but the difference did not reach significance (1.73 ± 0.88 versus 1.21 ± 0.92, Wilcoxon test,

$P = 0.06$). In the small metastatic tumor group, the mean CNR was significantly higher on T_1-Cube images

(2.06 ± 0.83 versus 1.05 ± 0.60; Wilcoxon test, $P < 0.01$).

Enhancement ratio

The mean CNR was significantly higher on T_1-Cube images than 3D FSPGR images for both the strong

enhancement group (1.78 ± 0.98 versus 1.25 ± 0.94; Wilcoxon test, $P < 0.05$) and weak enhancement group

$(1.90 \pm 0.95$ versus 1.12 ± 1.02; Wilcoxon test, $P < 0.01$) (Table 3).

Histopathological tumor type

As presented in Table 4, the mean CNR was also significantly higher on T_1-Cube images for the

metastasis group (2.14 ± 1.04 versus 1.23 ± 0.13; Wilcoxon test, $P < 0.01$) and lymphoma group (1.59 ± 0.52

versus 1.08 ± 0.36; Wilcoxon test, $P < 0.05$). In the HGG group, the mean CNR was also larger on T_1-Cube

images, but the difference did not reach statistical significance (1.31 ± 0.58 versus 0.91 ± 0.53; Wilcoxon test,

$P = 0.12$). In contrast, the mean CNR was almost the same for the meningioma group (1.68 ± 0.93 versus 1.71

± 0.86; Wilcoxon test, $P = 0.67$).

Discussion

In this study, we acquired T_1-Cube images before 3D FSPGR images because a longer delay after

injection of contrast agent results in greater enhancement, so 3D FSPGR images would be expected to exhibit

greater enhancement than T_1-Cube images. However, the overall mean CNR value and most tumor subtype

mean CNR values were higher on T_1-Cube images. The difference in mean CNR between T_1-Cube and 3D

FSPGR was especially great for smaller metastatic lesions (Figs. 2, 3). To the best of our knowledge, this is

the first study to demonstrate differences in contrast enhancement characteristics between T_1-Cube and 3D

FSPGR imaging using 3-T MR imaging.

Likewise, contrast enhancement was stronger on images obtained using T_1-SPACE, which also uses

variable flip angle T_1-weighted 3D spin-echo imaging, than on magnetization-prepared rapid gradient-echo

(MPRAGE) images.(9,10,13) Mugler and colleagues(2) reported higher tumor detectability using 2D T_1-weighted SE sequences than 3D T_1-weighted GRE sequences, and Yoshida's team(14) reported improved detection of small brain metastases using contrast-enhanced T_1-weighted volume isotropic turbo spin echo acquisition (T_1-VISTA). These results are generally consistent with ours using T_1-Cube 3-T MR imaging.

In analyses by tumor subtype, T_1-Cube images exhibited greater Gd enhancement than 3D FSPGR images for metastatic brain tumors and lymphoma, whereas mean CNR values did not differ significantly for HGG and meningiomas. The intrinsic reasons for these differences in CNR values among specific histological tumor types are not clear but may stem from differences in vascular permeability and/or extracellular space characteristics.

The reason for greater Gd enhancement by FSE-based T_1-Cube imaging than GRE-based 3D FSPGR imaging is also unclear, but numerous studies have reported this phenomenon.(1,2,15) Kato and associates(9) reported that SPACE sequences reduce the background signal via the magnetization transfer (MT) effect; specifically, a magnetization transfer prepulse suppresses the background signal for improved tumor enhancement. Similarly, the T_1-Cube sequence uses an FSE imaging technique in which multiple refocused pulses work as off-resonance pulses to provide an MT effect that reduces the background signal intensity from normal brain parenchyma. Nagao and colleagues(11) reported that turbo spin-echo (TSE) motion-sensitized driven-equilibrium (MSDE) prepulses suppress signals from small blood vessels to further enhance detectability. In addition, detection of dural or meningeal metastases appears better by FSE images than GRE images because FSE sequences tend to reduce signals from blood vessels at the brain surface, whereas such signals are usually hyperintense on 3D GRE images. Indeed, this effect obscured smaller lesions on 3D

FSPGR images in our study (Fig. 1, arrow).(9,16,17) As an alternative, the groups of Chen(18) and Fukuoka

(19) reported the greater sensitivity of 3D T_2 fluid-attenuated inversion recovery (T_2 FLAIR) than 3D T_1-

weighted imaging for detecting contrast enhancement. However, T_2 FLAIR requires time-consuming

acquisition of both pre- and post-contrast images.

Our study has several limitations. First, the number of cases was limited. Second, the scan time of T_1-

Cube was about 15% longer than that of 3D FSPGR, though our study analyzed CNRs, for which scan time

has relatively little influence. Several recent technical advances have contributed to a dramatic reduction in

scan time, including very long echo trains through refocusing FA (flip angle) modulation and 2D accelerated

parallel imaging, which may solve many problems associated with the protracted 3D FSE measurement

duration.(20,21) Third, other pathologies with enhancement, such as subacute infarction, may have

contaminated some of the enhancing lesions.

In conclusion, we found that Gd enhancement of the same heterogeneous population of tumors was higher

using T_1-Cube than 3D FSPGR, especially for smaller and weakly enhanced lesions, and suggest the

superiority of T_1-Cube to 3D FSPGR for the detection of small metastatic brain lesions.

References

1. Furutani K, Harada M, Mawlan M, Nishitani H. Difference in enhancement between spin echo and 3-dimensional fast spoiled gradient recalled acquisition in steady state magnetic resonance imaging of brain metastasis at 3-T magnetic resonance imaging. J Comput Assist Tomogr 2008; 32:313-319.

2. Mugler JP 3rd, Brookeman JR. Theoretical analysis of gadopentetate dimeglumine enhancement in T1-weighted imaging of the brain: comparison of two-dimensional spin-echo and three-dimensional gradient-echo sequences. J Magn Reson Imaging 1993; 3:761-769.

3. Li D, Haacke EM, Tarr RW, Venkatesan R, Lin W, Wielopolski P. Magnetic resonance imaging of the brain with gadopentetate dimeglumine-DTPA: comparison of T1-weighted spin-echo and 3D gradient-echo sequences. J Magn Reson Imaging 1996; 6:415-424.

4. Kakeda S, Korogi Y, Hiai Y, et al. Detection of brain metastasis at 3T: comparison among SE, IR-FSE and 3D-GRE sequences. Eur Radiol 2007; 17:2345-2351.

5. Pui MH, Fok EC. MR imaging of the brain: comparison of gradient-echo and spin-echo pulse sequences. AJR Am J Roentgenol 1995; 165:959-962.

6. Finelli DA, Hurst GC, Gullapalli RP. T1-weighted three-dimensional magnetization transfer MR of the brain: improved lesion contrast enhancement. AJNR Am J Neuroradiol 1998; 19:59-64.

7. Ai T, Zhang W, Priddy NK, Li X. Diagnostic performance of CUBE MRI sequences of the knee compared with conventional MRI. Clin Radiol 2012; 67:e58-e63.

8. Stanley DW, Kotsenas AL, Kaufmann TJ, et al. T1 CUBE compared to fast spin echo T1-weighted and BRAVO in post contrast enhanced brain MRI at 3T. In: Proceedings of the Joint Annual Meeting ISMRM-ESMRMB, Stockholm, Sweden. May 1-7, 2010 (4293)

9. Kato Y, Higano S, Tamura H, et al. Usefulness of contrast-enhanced T1-weighted sampling perfection with application-optimized contrasts by using different flip angle evolutions in detection of small brain metastasis at 3T MR imaging: comparison with magnetization-prepared rapid acquisition of gradient echo imaging. AJNR Am J Neuroradiol 2009; 30:923-929.

10. Reichert M, Morelli JN, Runge VM, et al. Contrast-enhanced 3-dimensional SPACE versus MP-RAGE

for the detection of brain metastases: considerations with a 32-channel head coil. Invest Radiol 2013; 48:55-60.

11. Nagao E, Yoshiura T, Hiwatashi A, et al. 3D turbo spin-echo sequence with motion-sensitized driven-equilibrium preparation for detection of brain metastases on 3T MR imaging. AJNR Am J Neuroradiol 2011; 32:664-670.

12. Rand S, Maravilla KR Schmiedl U. Lesion enhancement in radio-frequency spoiled gradient-echo imaging: theory, experimental evaluation, and clinical implications. AJNR Am J Neuroradiol 1994; 15:27-35.

13. Komada T, Naganawa S, Ogawa H, et al. Contrast-enhanced MR imaging of metastatic brain tumor at 3 tesla: utility of T_1-weighted SPACE compared with 2D spin echo and 3D gradient echo sequence. Magn Reson Med Sci 2008; 7:13-21.

14. Yoshida A, Tha KK, Fujima N, et al. Detection of brain metastases by 3-dimensional magnetic resonance imaging at 3 T: comparison between T1-weighted volume isotropic turbo spin echo acquisition and 3-dimensional T1-weighted fluid-attenuated inversion recovery imaging. J Comput Assist Tomogr 2013; 37:84-90.

15. Fishbach F, Bruhn H, Pech M, et al. Efficacy of contrast medium use for neuroimaging at 3.0 T: utility of IR-FSE compared to other T1-weighted pulse sequences. J Comput Assist Tomogr 2005; 29:499-505.

16. Mathews VP, Caldemeyer KS, Lowe MJ, Greenspan SL, Weber DM, Ulmer JL. Brain: gadolinium-enhanced fast fluid-attenuated inversion-recovery MR imaging. Radiology 1999; 211:257-263.

17. Mathews VP, Caldemeyer KS, Ulmer JL, Nguyen H, Yuh WT. Effect of contrast dose, delayed imaging, and magnetization transfer saturation on gadolinium-enhanced MR imaging of brain lesions. J Magn Reson Imaging 1997; 7:14-22.

18. Chen W, Wang L, Zhu W, et al. Multicontrast single-slab 3D MRI to detect cerebral metastasis. AJR Am J Roentgenol 2013; 198:27-32.

19. Fukuoka H, Hirai T, Okuda T, et al. Comparison of the added value of contrast-enhanced 3D fluid-attenuated inversion recovery and magnetization-prepared rapid acquisition of gradient echo sequences in relation to conventional postcontrast T1-weighted images for the evaluation of leptomeningeal diseases at 3T.

AJNR Am J Neuroradiol 2010; 31:868-873.

20. Busse RF, Brau AC, Vu A, et al. Effects of refocusing flip angle modulation and view ordering in 3D fast spin echo. Magn Reson Med 2008; 60:640-649.

21. Busse RF, Hariharan H, Vu A, Brittain JH. Fast spin echo sequences with very long echo trains: design of variable refocusing flip angle schedules and generation of clinical T2 contrast. Magn Reson Med 2006; 55:1030-1037.

Fig. 1. Defining regions of interest (ROIs) for calculation of contrast-to-noise ratio (CNR) and enhancement ratio (ER). Contrast-enhanced sagittal T_1-Cube image (a) and contrast-enhanced sagittal 3-dimensional (3D) fast spoiled gradient recall acquisition in steady state (FSPGR) image (b) showing the first ROI encompassing the lesion (ROI1) and the second encompassing a region of normal-appearing brain white matter close to the lesion (ROI2) for background subtraction. Note that the hyperintensity of superficial vessels on 3D FSPGR obscured lesions, whereas T_1-Cube suppressed signals from the vasculature (white arrow).

Fig. 2. Appearance of small, well enhanced lesions on a sagittal T_1-Cube image (a) and the corresponding sagittal 3-dimensional (3D) fast spoiled gradient recall acquisition in steady state (FSPGR) image (b). Multiple small and well enhanced lesions are more clearly revealed on the T_1-Cube image than on the 3D FSPGR image (arrows).

Fig. 3. Appearance of small, weakly enhanced lesions on an axial T_1-Cube image (a) and the corresponding axial 3-dimensional (3D) fast spoiled gradient recall acquisition in steady state (FSPGR) image (b). Numerous weakly enhanced lesions are well delineated by T_1-Cube. These lesions were uniformly fainter on 3D FSPGR, and one small nodular lesion was barely detectable above the background on 3D FSPGR (arrow).

Table 1. Patient demographics and diagnosis

Patient	Age (years)	Sex	Diagnosis	No. of Lesions
1	48	F	Metastasis from breast cancer	13
2	63	M	Metastasis from gastric cancer	1
3	72	M	Metastasis from colon cancer	1
4	70	F	Metastasis from colon cancer	8
5	57	M	Metastasis from lung cancer	2
6	77	M	Metastasis from lung cancer	6
7	68	M	Metastasis from lung cancer	1
8	59	F	Metastasis from lung cancer	1
9	81	M	Metastasis from RCC	1
10	39	F	Meningioma	1
11	84	F	Meningioma	1
12	39	F	Meningioma	1
13	70	F	Meningioma	1
14	59	M	Meningioma	1
15	61	F	Meningioma	1
16	70	F	Meningioma	1
17	81	M	Hemangiopericytoma	1
18	45	M	AO, WHO grade III	1
19	41	M	AA, WHO grade III	1
20	54	F	AA, WHO grade III	1
21	72	F	GBM, WHO grade IV	1
22	34	M	GBM, WHO grade IV	1
23	84	F	GBM, WHO grade IV	1
24	53	M	GBM, WHO grade IV	1
25	72	M	GBM, WHO grade IV	3
26	59	M	GBM, WHO grade IV	1
27	61	M	GBM, WHO grade IV	1
28	82	F	GBM, WHO grade IV	1
29	73	M	DLBCL	1

30	59	M	DLBCL	1
31	55	F	DLBCL	3
32	78	F	DLBCL	1

AA, anaplastic astrocytoma; AO, anaplastic oligodendroglioma; DLBCL, diffuse large B-cell lymphoma; GBM, glioblastoma multiforme; RCC, renal cell carcinoma; WHO, World Health Organization

Intracranial tumors in all except 2 patients were diagnosed by histology. The remaining 2 meningiomas in Cases 10 and 12 were diagnosed by imaging.

Table 2. Comparison of contrast-to-noise ratio (CNR) measured by T_1-Cube and then 3-dimensional (3D) fast spoiled gradient recall acquisition in steady state (FSPGR) for large and small metastatic tumors

	T_1-Cube	3D FSPGR	*P* value
Large metastatic tumor	1.73 ± 0.88	1.21 ± 0.92	0.06
Small metastatic tumor	2.06 ± 0.83	1.05 ± 0.60	< 0.01

Data are mean ± standard deviation (SD) for 17 lesions (large metastatic tumor group) and 17 lesions (small metastatic tumor group).

Table 3. Comparison of contrast-to-noise ratio (CNR) measured by T_1-Cube and then 3-dimensional (3D) fast spoiled gradient recall acquisition in steady state (FSPGR) for strong and weak enhancement groups

	T_1-Cube	3D FSPGR	P value
Strong enhancement group	1.78 ± 0.98	1.25 ± 0.94	< 0.05
Weak enhancement group	1.90 ± 0.95	1.12 ± 1.02	< 0.01

Data are mean $\pm$ standard deviation (SD) for 28 strongly enhanced lesions and 33 weakly enhanced lesions.

Table 4. Comparison of contrast-to noise ratio (CNR) measured by T_1-Cube and then 3-dimensional (3D) fast spoiled gradient recall acquisition in steady state (FSPGR) for different histopathological tumor groups

	T_1-Cube	3D FSPGR	P value
Metastasis	2.14 ± 1.04	1.23 ± 0.13	< 0.01
High grade glioma	1.31 ± 0.58	0.91 ± 0.53	0.12
Meningioma	1.68 ± 0.93	1.71 ± 0.86	0.67
Lymphoma	1.59 ± 0.52	1.08 ± 0.36	< 0.05

Data are mean $\pm$ standard deviation (SD) for 34 lesions (metastasis), 13 lesions (high grade glioma), 8 lesions (meningioma), and 6 lesions (lymphoma).
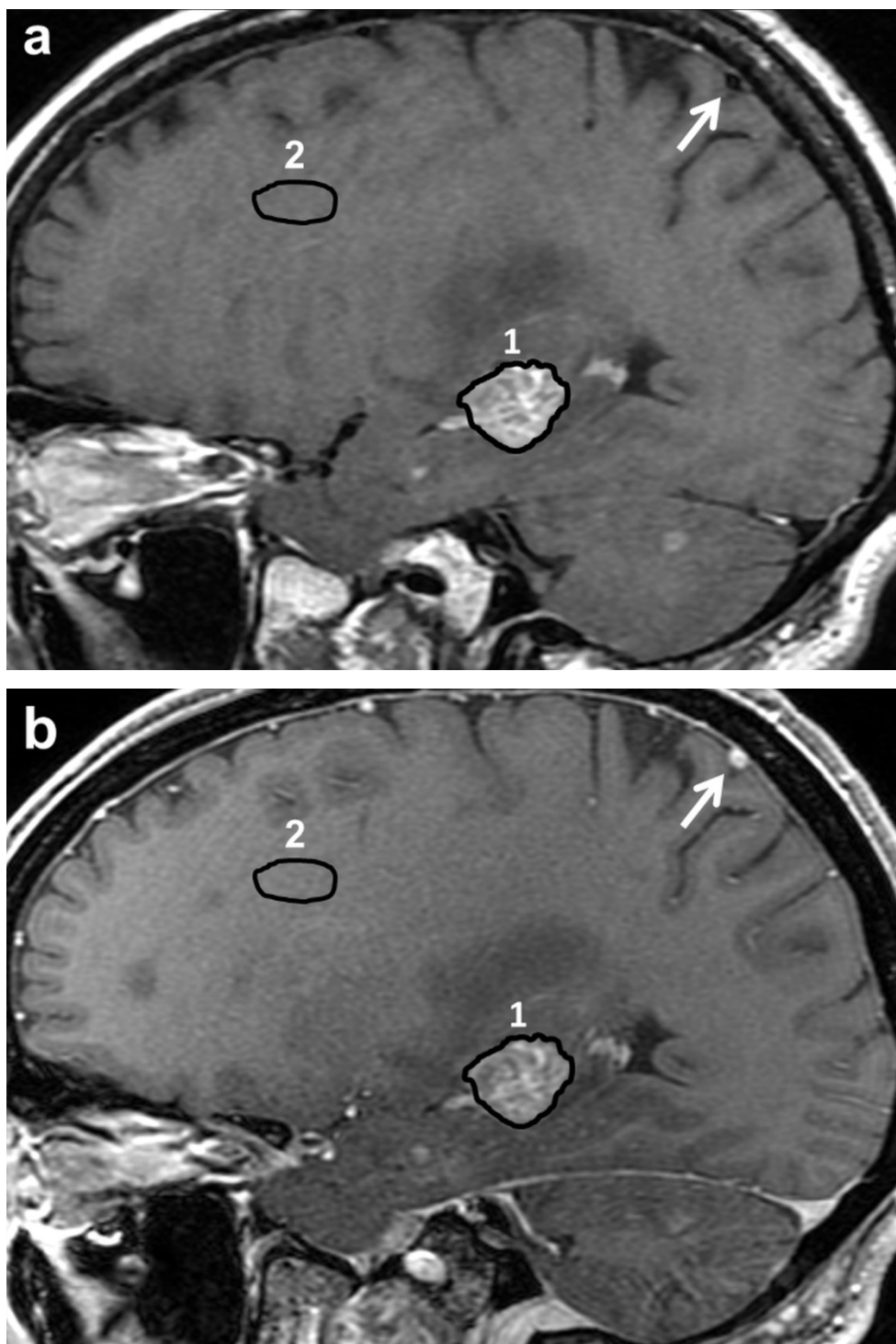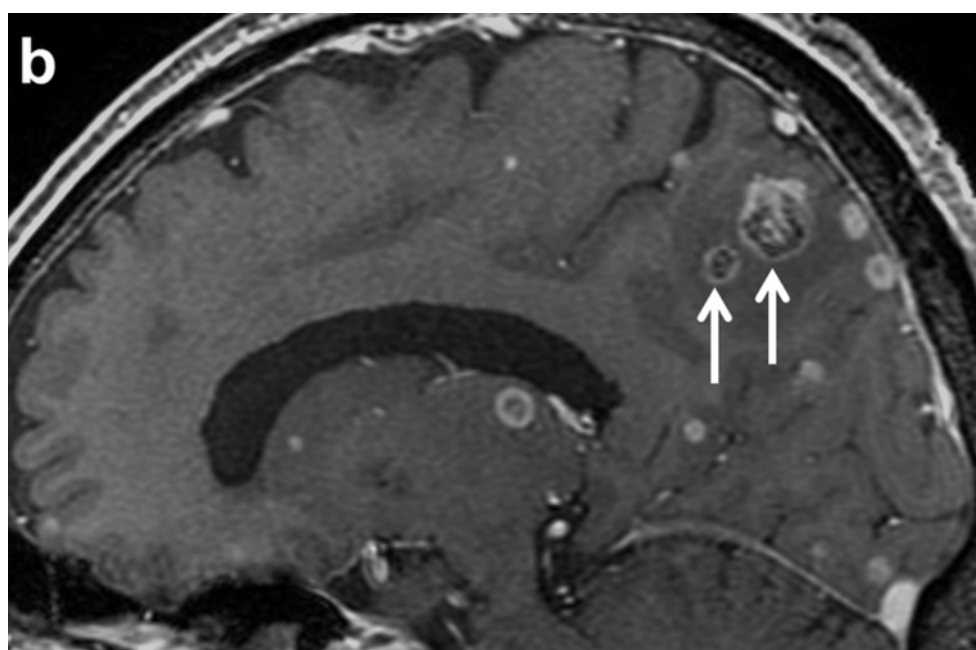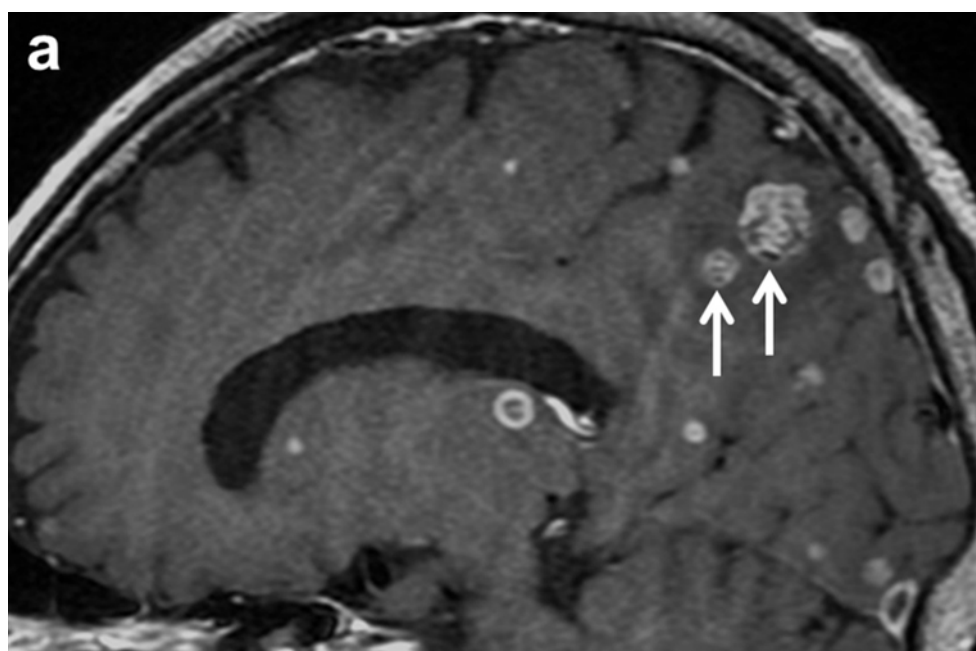
Figures

Figure 1

Figure 2

Figure 3